THE JOURNAL OF PHYSICAL CHEMISTRY B

Article

pubs.acs.org/JPCB

Vapor–Liquid Equilibrium and Polarization Behavior of the GCP Water Model: Gaussian Charge-on-Spring versus Dipole Self-Consistent Field Approaches to Induced Polarization

Ariel A. Chialvo,*[,†] Filip Moucka,[‡] Lukas Vlcek,[†,§] and Ivo Nezbeda[‡,∥]

[†]Chemical Sciences Division, Geochemistry and Interfacial Sciences Group, Oak Ridge National Laboratory, Oak Ridge, Tennessee 37831-6110, United States

[‡]Faculty of Science, J. E. Purkinje University, 40096 Usti nad Labem, Czech Republic

[§]Joint Institute for Computational Sciences, Oak Ridge National Laboratory, Oak Ridge, Tennessee 37831-6173, United States

[∥]E. Hala Laboratory of Thermodynamics, Institute of Chemical Process Fundamentals Academy of Sciences, 16502 Prague 6, Czech Republic

ABSTRACT: We developed the Gaussian charge-on-spring (GCOS) version of the original self-consistent field implementation of the Gaussian Charge Polarizable water model and test its accuracy to represent the polarization behavior of the original model involving smeared charges and induced dipole moments. For that purpose we adapted the recently proposed multiple-particle-move (MPM) within the Gibbs and isochoric-isothermal ensembles Monte Carlo methods for the efficient simulation of polarizable fluids. We assessed the accuracy of the GCOS representation by a direct comparison of the resulting vapor–liquid phase envelope, microstructure, and relevant microscopic descriptors of water polarization along the orthobaric curve against the corresponding quantities from the actual GCP water model.

I. INTRODUCTION

Water modeling has gone a long way since the inspiring initial steps by Ben-Naim and Stillinger[1] who illustrated that it was possible to capture the complex behavior of water through a judicious description of the system Hamiltonian involving just a few adjustable (force field) parameters.[2−7] Considering the highly polarizable nature of water and its notorious anomalous properties it becomes clear that water modeling has made remarkable advances from the original nonpolarizable descriptions toward the microscopic understanding of the macroscopic behavior. While there are still developments involving nonpolarizable models,[8−11] the modeling community has reached a consensus on the need for the explicit introduction of induced polarization to improve the quantitative agreement between the model description and the real behavior of water.[12−20]

One relevant target for the test of accuracy/realism of a model is the description of the vapor–liquid equilibrium (VLE) envelope, which usually translates into the direct determination of the two phases in equilibrium via temperature-quenching,[21,22] grand canonical Monte Carlo (GCMC) with histogram reweighing,[23] Gibbs Ensemble Monte Carlo (GEMC),[24] and Gibbs Ensemble molecular dynamics (GEMD)[25−28] simulations (in addition to Gibbs–Duhem integration[29] whenever one coexistence point is already known). Because the equivalence among these techniques is well established, the choice of one over the other for nonpolarizable water models is not that crucial since all of them involve pairwise additive interactions. The real challenge resides in the determination of orthobaric conditions for polarizable water (or any other polarizable fluid for that matter) models via conventional "single particle move" Monte Carlo approaches, in that, the CPU-time requirement for attaining an equilibrium state for a polarizable model scales as $\sim N^2$, that is, $\sim N$ larger than that for the corresponding nonpolarizable counterpart characterize by a number of molecules N.

While there has been several attempts to reduce such computational burden in the implementation of the GEMC for polarizable water models[30−32] while keeping its intrinsic "single particle move" nature, these methods have been shown to yield, when implemented with a careful choice of simulation parameters, an identical outcome to those from rigorous matrix minimization.[33,34] Otherwise, these methods might introduce unacceptable biased sampling for some models as we have discussed previously in the application ANES-MC and PAPI to treat induced dipole polarization in water,[35] while others trade computational efficient at the expense of accuracy.[36] Moucka et al.[36−39] have recently developed and implemented a "multiple particle move" Monte Carlo approach to reduce the computational requirement, and consequently, increase the efficiency of the configurational sampling in Monte Carlo scheme for nonpolarizable and polarizable models alike.

Another relevant issue regarding the molecular simulation of polarizable model involving Gaussian electrostatics is dealing with the complications arising from the self-consistent

Received: January 20, 2015
Revised: March 21, 2015
Published: March 24, 2015

DOI: 10.1021/acs.jpcb.5b00595
J. Phys. Chem. B 2015, 119, 5010−5019

determination of induced dipole moments and the corresponding induced dipole−induced dipole as well as charge-induced dipole interactions (vide infra and Appendix A of ref 40). Although the induced dipole formalism is perhaps the most obviously rigorous way to model species polarizability,[41,42] and is being successfully implemented in the simulation of aqueous and organic systems,[2,43−45] this approach is not the preferred scheme when comes to incorporating induced polarization into standard simulation packages. In fact, different variations of "charge on a spring" (COS)[46,47] or classical "Drude oscillator"[48] models are becoming more frequently used to describe the electronic induction in terms of the displacement of massless charges,[49] attached by harmonic springs to the polarizable sites, under the effect of the local electric field.[50−52] Moreover, while most COS models are based on point-charge electrostatics[16,47] and have been implemented in a number of popular molecular dynamics simulation packages, including NAMD,[53] CHARMM,[54] and DL_POLY,[55] a recent polarizable water modeling has successfully implemented a COS approach involving Gaussian rather than point charges.[56,57]

The above scenario suggests addressing a relevant issue, which becomes the main goal of this work: How equivalent are the descriptions of the polarization behavior of the Gaussian Polarizable Charge (GCP) water model under the self-consistent field implementation of the Gaussian induced dipole polarization and its Gaussian charge-on-spring (GCOS) counterpart? To address this issue and test such equivalence in the description of induced-dipole polarization, we first determine the model's vapor−liquid coexistence envelope based on MPM-GEMC simulations for the GCOS version of the GCP water model. Then, we study the behavior of some relevant polarization parameters including the average total dipole moment, its average induced dipole component, as well as the average angle between the permanent and the induced dipoles at states along the orthobaric density curve. Finally, we study the corresponding water microstructure in terms of radial distribution functions for selected states, and discuss the choice of the magnitude of the Gaussian Drude charge in the GCOS implementation.

For that purpose the layout of the manuscript is as follows. In section II we provide a brief description of the GCP water model with the underlying dipole self-consistent field (SCF) solution of the implicit induced-dipole equation and the proposed GCOS version. In section III we describe the simulation methodology underlying the molecular dynamics of the GCP water model and the MPM-MC of the corresponding GCOS implementation. In section IV we address the accuracy of the GCOS representation through the direct comparison between representative simulated properties, including the vapor−liquid phase envelope, microstructure, and water polarization along the orthobaric curve, and the corresponding quantities from the actual GCP water model. Finally, we close with a brief discussion of relevant conclusions.

II. GAUSSIAN CHARGE POLARIZABLE MODEL

The Gaussian charge polarizable water model, in its original reaction field[58,59] or recent Ewald summation implementations,[40] comprises van der Waals (nonelectrostatic) interactions, Gaussian charges, and corresponding induced-dipole moments to account for the electrostatic interactions. The van der Waals intermolecular interactions between the oxygen sites of water are described by a soft-repulsive version of the exponential-6 potential, to avoid potential issues[60] associated with the divergence of $\phi_{\mathrm{buck}}(r_{\mathrm{OO}} < r_{\mathrm{M}})$, where r_{M} is the smallest root of $[\partial\phi_{\mathrm{buck}}(r_{\mathrm{OO}})/\partial r_{\mathrm{OO}}]_{r_{\mathrm{OO}}=r_{\mathrm{M}}} = 0$, that is,

$$U_{\mathrm{vdw}} = \sum_{i<j=1,N} \phi_{m\_\exp 6}(r_{\mathrm{OO}}) \tag{1}$$

where the subscript "buck" refers to the original Buckingham potential,[61] that is,

$$\phi_{\mathrm{buck}}(r_{\mathrm{OO}}) = \left(\frac{\varepsilon_{\mathrm{OO}}}{1 - 6/\gamma_{\mathrm{OO}}}\right)[(6/\gamma_{\mathrm{OO}})\exp(\gamma_{\mathrm{OO}} \times [1 - (r_{\mathrm{OO}}/\sigma_{\mathrm{OO}})]) - (\sigma_{\mathrm{OO}}/r_{\mathrm{OO}})^6] \tag{2}$$

Thus, the oxygen−oxygen pair interaction follows a continuous representation described as follows:[60]

$$\phi_{m\_\exp 6}(r_{\mathrm{OO}}) = \begin{cases} \phi_{\mathrm{buck}}(r_{\mathrm{OO}}) & \text{if } r_{\mathrm{c}} > r_{\mathrm{OO}} > r_{\mathrm{M}} \\ -\phi_{\mathrm{buck}}(r_{\mathrm{OO}}) + 2\phi_{\mathrm{buck}}(r_{\mathrm{M}}) & \text{if } r_{\mathrm{OO}} \le r_{\mathrm{M}} \end{cases} \tag{3}$$

with $r_{\mathrm{c}} \le 0.5L$ as the cutoff truncation radius consistent with the simulation box-size L, and r_{M} is the root of the transcendental equation $\exp(\gamma_{\mathrm{OO}}[1 - (r_{\mathrm{M}}/\sigma_{\mathrm{OO}})]) - (\sigma_{\mathrm{OO}}/r_{\mathrm{M}})^7 = 0$.

The electrostatic energy of the aqueous electrolyte solution involving Gaussian partial charges and induced dipole moments is described in terms of the interaction and polarization contributions as follows:[19]

$$U_{\mathrm{el}} = U_{\mathrm{int}} + U_{\mathrm{pol}} \tag{5}$$

Specifically, for our model system characterized by the Gaussian charge distribution $\rho^{\alpha}_{q_i}(r)$ for the α-site partial-charge q_i^{α},

$$\rho_{q_i^{\alpha}}(r) = [q_i^{\alpha}/(2\pi\sigma_{\alpha}^2)^{1.5}]\exp[-|\boldsymbol{r} - \boldsymbol{r}_{i_\alpha}|^2/2\sigma_{\alpha}^2] \tag{6}$$

and the center of mass Gaussian dipole-charge distribution $\rho_{\mu i}(r)$ for the induced dipole $\boldsymbol{\mu}_i^{\mathrm{ind}}$,

$$\rho_{\mu_i}(r) = [\boldsymbol{\mu}_i^{\mathrm{ind}}\cdot\nabla_i/(2\pi\sigma_{\mu}^2)^{1.5}]\exp[-|\boldsymbol{r} - \boldsymbol{r}_i|^2/2\sigma_{\mu}^2] \tag{7}$$

the "int" contribution to eq 5 can be written as $U_{\mathrm{int}} = U_{qq} + U_{q\mu} + U_{\mu\mu}$, that is, in terms of the charge−charge, charge−induced dipole, and induced dipole−induced dipole interactions, respectively.[62] More explicitly, these contributions are given by (see Appendix A of the SI document of ref 40 for details),

$$U_{qq} = \sum_{i<j}\sum_{\alpha,\beta} q_i^{\alpha} q_j^{\beta} \hat{T}_{i_\alpha j_\beta}(r_{i_\alpha j_\beta}) \tag{8}$$

$$U_{q\mu} = \sum_{i<j}\sum_{\alpha,\beta} (-q_i^{\alpha}\hat{T}^{\gamma}_{i_\alpha j}(r_{i_\alpha j})\mu_j^{\mathrm{ind},\gamma} + \mu_i^{\mathrm{ind},\gamma}\hat{T}^{\gamma}_{ij_\beta}(r_{ij_\beta})q_j^{\beta}) \tag{9}$$

$$U_{\mu\mu} = \sum_{i<j} \mu_i^{\mathrm{ind},\alpha}\hat{T}_{ij}^{\alpha\beta}(r_{ij})\mu_j^{\mathrm{ind},\beta} \tag{10}$$

involving the following Cartesian operators $\hat{T}(r) \equiv erf(\kappa r)/r$, $\hat{T}^{\gamma}(r) \equiv \nabla_{\gamma}\hat{T}(r)$, and $\hat{T}^{\gamma\lambda}(r) \equiv \nabla_{\lambda}\hat{T}^{\gamma}(r)$, whose explicit expressions are given in eqs 11−13 of ref 40, with $\kappa_{\beta} = (\sigma_{\beta}\sqrt{2})^{-1}$ and σ_{β} denoting the width of the corresponding Gaussian distribution.

Finally, the polarization contribution in eq 5 results from the equilibrium condition $\partial U_{\mathrm{el}}/\partial\boldsymbol{\mu}_i^{\mathrm{ind}} = \partial U_{\mathrm{el}}/\partial\boldsymbol{E}_i^{\mathrm{tot}} = 0$,[62] that is,

DOI: 10.1021/acs.jpcb.5b00595
J. Phys. Chem. B 2015, 119, 5010−5019

$$U_{\mathrm{pol}} = 0.5 \sum_i (\boldsymbol{\mu}_i^{\mathrm{ind}} \cdot \boldsymbol{\mu}_i^{\mathrm{ind}})/\alpha_i \tag{11}$$

where the induced dipole moment $\boldsymbol{\mu}_i^{\mathrm{ind}}$ at the center of mass of the i particle is given by the self-consistent solution of the $\boldsymbol{\mu}_i^{\mathrm{ind}}$, implicit equation,

$$\boldsymbol{\mu}_i^{\mathrm{ind}} = \alpha_i \boldsymbol{E}_i^{\mathrm{tot}}(\{\boldsymbol{\mu}_{i=1,N}^{\mathrm{ind}}\}) \tag{12}$$

that is, the result of the interaction between the total electric field $\boldsymbol{E}_i^{\mathrm{tot}} = \boldsymbol{E}_i^{qq} + \boldsymbol{E}_i^{\mu\mu}$ and the isotropic polarizability α_i. Note that we use the notation $\boldsymbol{E}_i^{\mathrm{tot}}(\{\boldsymbol{\mu}_{i=1,N}^{\mathrm{ind}}\})$ to highlight the implicit nature of eq 12 through the induced electric field $\boldsymbol{E}_i^{\mu\mu}(\{\boldsymbol{\mu}_{i=1,N}^{\mathrm{ind}}\})$.

Under this framework, water comprises a planar rigid geometry with three atomic masses for the oxygen (O) and hydrogen (H) sites, and two additional for the location of massless site (M) and the molecular center of mass where we locate the isotropic polarizability α_i = 1.444 Å^3. The O−H bonds with a length l_{OH} = 0.9572 Å define the angle ∠HOH = 104.52° and the M-site located, at a distance l_{OM} = 0.27 Å from the O-site along the ∠HOH bisector, bears the negative Gaussian electrostatic charge with a magnitude $q_{\mathrm{M}} = -2q_{\mathrm{H}} = -1.2226e$, resulting in a permanent dipole moment of 1.85D.

Gaussian Charge-on-Spring Approach to the Induced Dipole in the GCP Modeling. For the GCOS version of the GCP, we substitute the calculation of the induced dipole moments, eq 12, with that resulting from the oscillating displacement of two Gaussian charges $\rho_{q_{\mathrm{D}_{i'}}^{(\alpha)}}(r) = [\pm q_{\mathrm{D}_{i'}}^{(\alpha)}/(2\pi\sigma_{\mathrm{D}}^2)^{1.5}]\exp[-|\boldsymbol{r} - \boldsymbol{r}_i|^2/2\sigma_{\mathrm{D}}^2]$ of magnitude $2e \le |q_{\mathrm{D}_{i'}}^{(\alpha)}| \le 10e$ (whose choice will be discussed below), attached to the water's center of mass by two springs with a force-constant $(|q_{\mathrm{D}_{i'}}^{(\alpha)}|^2/\alpha_i)$, that is, rendering the entire molecule electroneutral. Under these conditions, the relevant contributions to the configurational energy become

$$U_{\mathrm{D}} = U_{qq} + U_{\mathrm{self}} \tag{13}$$

where $U_{\mathrm{self}} = 0.5k_{\mathrm{D}}\sum_i (l_{i_1}^2 + l_{i_2}^2)$, l_{i_α} denotes the displacement of the α-Drude charge, $q_{\mathrm{D}_{i'}}^{(\alpha)}$, from the center of mass of the i-molecule, and U_{qq} comprises three terms describing the Gaussian charge-Gaussian charge interactions, that is,

$$\begin{aligned} U_{qq}^{\mathrm{GCOS}} = & \sum_{i<j}\sum_{\alpha,\beta} q_i^\alpha q_j^\beta \,\mathrm{erf}(\kappa_{\alpha\beta} r_{i_\alpha j_\beta})/r_{i_\alpha j_\beta} \\ & + \sum_{i<j'}\sum_{\alpha,\beta} q_i^\alpha q_{\mathrm{D}_{j'}}^{(\beta)} \,\mathrm{erf}(\kappa_{\alpha\mathrm{D}} r_{i_\alpha j_{\beta'}})/r_{i_\alpha j_{\beta'}} \\ & + \sum_{i'<j'}\sum_{\alpha,\beta} q_{\mathrm{D}_{i'}}^{(\alpha)} q_{\mathrm{D}_{j'}}^{(\beta)} \,\mathrm{erf}(\kappa_{\mathrm{DD}} r_{i_{\alpha'} j_{\beta'}})/r_{i_{\alpha'} j_{\beta'}} \end{aligned} \tag{14}$$

where the primed coordinates refer to the Drude Gaussian charge, that is, $\boldsymbol{r}_{i_{\alpha'}} = \boldsymbol{r}_i + \boldsymbol{l}_{i_\alpha}$. Thus, for any configuration of N polarizable water molecules, the equilibrium condition of the Drude oscillators is given by the condition

$$\partial U_{\mathrm{D}}/\partial l_{i_\alpha} = k_{\mathrm{D}} l_{i_\alpha} - q_{\mathrm{D}_{i'}}^{(\alpha)} \boldsymbol{E}_{i_\alpha}^{\mathrm{tot}}(\{\boldsymbol{\mu}_{i=1,N}^{\mathrm{ind}}\}) = 0, \quad \alpha = 1, 2 \tag{15}$$

where $\boldsymbol{E}_{i_\alpha,\gamma}^{\mathrm{tot}}(\{\boldsymbol{\mu}_{i=1,N}^{\mathrm{ind}}\}) = -(\sum_{j\neq i_\alpha}\sum_\beta \hat{T}_{i_\alpha j_\beta}^\gamma (r_{i_{\alpha'} j_\beta}) q_j^\beta + \sum_{j_{\beta'}\neq i_\alpha}\sum_\beta \hat{T}_{i_\alpha j_{\beta'}}^\gamma (r_{i_\alpha j_{\beta'}}) q_{\mathrm{D}_{j'}}^{(\beta)})$ is the γ-component of the total electric field generated by all electrostatic charges (i.e., q_{M}, q_{H}, and $q_{\mathrm{D}_{i'}}^{(\alpha)}$) around the equilibrium position l_{i_α} of the Drude charge $q_{\mathrm{D}_{i'}}^{(\alpha)}$ with respect to the center of mass of the water molecule. Because $q_{\mathrm{D}_{i'}}^{(1)} = -q_{\mathrm{D}_{i'}}^{(2)}$, eq 15 indicates that

$$\begin{aligned} k_{\mathrm{D}} l_{i_1} &= q_{\mathrm{D}}^{(1)} \boldsymbol{E}_{i_1}^{\mathrm{tot}}(\{\boldsymbol{\mu}_{i=1,N}^{\mathrm{ind}}\}) \\ k_{\mathrm{D}} l_{i_2} &= -q_{\mathrm{D}}^{(1)} \boldsymbol{E}_{i_2}^{\mathrm{tot}}(\{\boldsymbol{\mu}_{i=1,N}^{\mathrm{ind}}\}) \end{aligned} \tag{16}$$

so that $k_{\mathrm{D}}(l_{i_1} - l_{i_2}) = q_{\mathrm{D}_{i'}}^{(1)}[\boldsymbol{E}_{i_1}^{\mathrm{tot}}(\{\boldsymbol{\mu}_{i=1,N}^{\mathrm{ind}}\}) - \boldsymbol{E}_{i_2}^{\mathrm{tot}}(\{\boldsymbol{\mu}_{i=1,N}^{\mathrm{ind}}\})]$

Now, we can either assume that $\boldsymbol{E}_{i_\alpha}^{\mathrm{tot}}(\{\boldsymbol{\mu}_{i=1,N}^{\mathrm{ind}}\}) \simeq \boldsymbol{E}_i^{\mathrm{tot}}(\{\boldsymbol{\mu}_{i=1,N}^{\mathrm{ind}}\})$ for small values of the Drude displacement $|l_{i_\alpha}|$ or invoke the condition $\lim_{|l_{i_1}|\to 0} \boldsymbol{E}_{i_1}^{\mathrm{tot}}(\{\boldsymbol{\mu}_{i=1,N}^{\mathrm{ind}}\}) = \boldsymbol{E}_i^{\mathrm{tot}}(\{\boldsymbol{\mu}_{i=1,N}^{\mathrm{ind}}\})$, so that, from eq 16, we have that $l_{i_1} = -l_{i_2}$, $\boldsymbol{\mu}_i^{\mathrm{ind}} = (l_{i_1} - l_{i_2})q_{\mathrm{D}_{i'}}^{(1)} = 2l_{i_1}q_{\mathrm{D}_{i'}}^{(1)}$, and consequently,

$$\boldsymbol{\mu}_i^{\mathrm{ind}} = (2q_{\mathrm{D}}^2/k_{\mathrm{D}})\boldsymbol{E}_i^{\mathrm{tot}}(\{\boldsymbol{\mu}_{i=1,N}^{\mathrm{ind}}\}) \tag{17}$$

with $q_{\mathrm{D}} = |q_{\mathrm{D}_{i'}}^{(1)}|$, and according to eq 12, the spring force-constant follows the relation $k_{\mathrm{D}} \equiv 2q_{\mathrm{D}}^2/\alpha_i$.

Link between GCOS and Self-Consistent Induced Dipole Approaches to GCP Modeling. Here we illustrate the theoretical equivalence between the self-consistent induced dipole and the charge-on-spring implementation of induced polarization involving Gaussian charges in the modeling of GCP water[40] by rewriting eq 14 in an equivalent and more general form. This alternative form becomes handy to draw some parallels with other modeling efforts involving GCOS schemes. In principle, we could attach Drude charges to all four relevant sites of the GCP water model, that is,

$$\begin{aligned} U_{qq} = & \sum_{i<j}\sum_{\alpha,\beta} (q_i^\alpha - q_{\mathrm{D}_i}^{(\alpha)})(q_j^\beta - q_{\mathrm{D}_j}^{(\beta)})\,\mathrm{erf}(\kappa_{\alpha\beta} r_{i_\alpha j_\beta})/r_{i_\alpha j_\beta} \\ & + \sum_{i<j'}\sum_{\alpha,\beta} (q_i^\alpha - q_{\mathrm{D}_i}^{(\alpha)}) q_{\mathrm{D}_{j'}}^{(\beta)} \,\mathrm{erf}(\kappa_{\alpha\mathrm{D}} r_{i_\alpha j_{\beta'}})/r_{i_\alpha j_{\beta'}} \\ & + \sum_{i'<j}\sum_{\alpha,\beta} q_{\mathrm{D}_{i'}}^{(\alpha)} (q_j^\beta - q_{\mathrm{D}_j}^{(\beta)})\,\mathrm{erf}(\kappa_{\beta\mathrm{D}} r_{i_{\alpha'} j_\beta})/r_{i_{\alpha'} j_\beta} \\ & + \sum_{i'<j'}\sum_{\alpha,\beta} q_{\mathrm{D}_{i'}}^{(\alpha)} q_{\mathrm{D}_{j'}}^{(\beta)} \,\mathrm{erf}(\kappa_{\mathrm{DD}} r_{i_{\alpha'} j_{\beta'}})/r_{i_{\alpha'} j_{\beta'}} \end{aligned} \tag{18}$$

with $1 \le \alpha, \beta \le 4$, and still recover eq 14 due to molecular electroneutrality, by recalling that the GCP water model does not carry any charge at the center of mass, while neither the M-site nor the hydrogen sites are polarizable (Figure 1, left). For the case of the GCP water model the Drude charges are $q_{\mathrm{D}_a}^{(\alpha)} = \pm q_{\mathrm{D}}$, with $a = (i', j')$ and $\alpha = (1, 2)$, that is, connected to the molecular center of mass of molecule (Figure 1, right). In

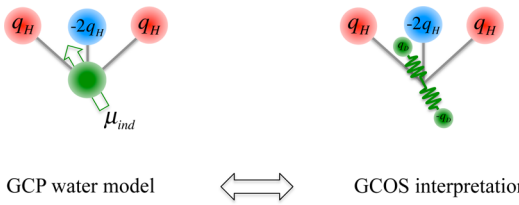

Figure 1. Schematics of the GCP water model and its GCOS counterpart.

DOI: 10.1021/acs.jpcb.5b00595
J. Phys. Chem. B 2015, 119, 5010−5019

addition, we impose the condition that the amplitude of the Drude's charge displacement be small enough so that $|l_{i_\alpha}| \ll |r_{i_\alpha j_\beta}|$. Under these conditions, we can rewrite it in terms of a multipole expansion around the molecule's center of mass as follows:[63]

$$U_{qq} \simeq \sum_{i<j}\sum_{\alpha,\beta} q_i^\alpha q_j^\beta \hat{T}_{i_\alpha j_\beta}(r_{i_\alpha j_\beta}) - \sum_{i<j'}\sum_{\alpha,\beta} q_i^\alpha \hat{T}^\gamma_{i_\alpha j_{\beta'}}(r_{i_\alpha j_{\beta'}}) q^{(\beta)}_{\mathrm{D}_{j'}} l^\gamma_{j_\beta} + \sum_{i'<j}\sum_{\alpha,\beta} q^{(\alpha)}_{\mathrm{D}_{i'}} l^\gamma_{i_\alpha} \hat{T}^\gamma_{i_\alpha j_\beta}(r_{i_\alpha j_\beta}) q_j^\beta + \sum_{i'<j'}\sum_{\alpha,\beta} q^{(\alpha)}_{\mathrm{D}_{i'}} l^\gamma_{i_\alpha} \hat{T}^{\gamma\lambda}_{i_\alpha j_{\beta'}}(r_{i_\alpha j_{\beta'}}) q^{(\beta)}_{\mathrm{D}_{j'}} l^\lambda_{j_\beta} \tag{19}$$

where the operators $\hat{T}(r) \equiv \mathrm{erf}(\kappa r)/r$, $\hat{T}^\gamma(r) \equiv \nabla_\gamma \hat{T}(r)$, and $\hat{T}^{\gamma\lambda}(r) \equiv \nabla_\lambda \hat{T}^\gamma(r)$, with $\nabla_\gamma(\cdots) \equiv [\partial(\cdots)/\partial \boldsymbol{r}]_\gamma$ were described previously.[40] Moreover, eq 15 now becomes

$$k_{\mathrm{D}} l_{i_\alpha} + \sum_{i'\neq j}\sum_{\beta} q^{(\alpha)}_{\mathrm{D}_{i'}} \hat{T}^\gamma_{i_\alpha j_\beta}(r_{i_\alpha j_\beta}) q_j^\beta - \sum_{i'\neq j'}\sum_{\beta} q^{(\alpha)}_{\mathrm{D}_{i'}} \hat{T}^{\gamma\lambda}_{i_\alpha j_{\beta'}}(r_{i_\alpha j_{\beta'}}) q^{(\beta)}_{\mathrm{D}_{j'}} l^\lambda_{j_\beta} = 0 \tag{20}$$

where we can substitute k_{D} with its equivalent $(2q_{\mathrm{D}}^2/\alpha_i)$ so that eq 20 reduces to the familiar expression

$$2q^{(\alpha)}_{\mathrm{D}_{i'}} l_{i_\alpha}/\alpha_i + \sum_{i'\neq j}\sum_{\beta} \hat{T}^\gamma_{i_\alpha j_\beta}(r_{i_\alpha j_\beta}) q_j^\beta - \sum_{i'\neq j'}\sum_{\beta} \hat{T}^{\gamma\lambda}_{i_\alpha j_{\beta'}}(r_{i_\alpha j_{\beta'}}) q^{(\beta)}_{\mathrm{D}_{j'}} l^\lambda_{j_\beta} = 0 \tag{21}$$

which is eq 12 since $\boldsymbol{\mu}_i^{\mathrm{ind}} = 2l_{i_\alpha} q^{(\alpha)}_{\mathrm{D}_{i'}}$. For a representative maximum induced dipole moment of $|\boldsymbol{\mu}_i^{\mathrm{ind}}| = 2.0$ D, typically found in very extreme water environments,[20] and $2e \le |q_{\mathrm{D}}| \le 10e$, the largest displacement becomes $0.04 \le |l_{i_\alpha}| \le 0.2$ Å, which obviously satisfies the required $|l_{i_\alpha}| \ll |r_{i_\alpha j_\beta}|$ condition.

III. SIMULATION METHODOLOGY

All molecular dynamics simulations of the GCP water model were performed at isochoric-isothermal conditions, either in the reaction field[59] or the Ewald implementation,[40] using $N = 256$ molecules in a cubic box at the orthobaric state conditions previously determined by GEMC (see Table 8 of ref 59.) where the isothermal conditions were achieved through independent Nosé thermostats for the rotational and translational degrees of freedom.[64,65] For the integration of the Newton-Euler equations of motion we used a fourth-order Gear's predictor-corrector algorithms for the translational degrees of freedom (2nd order ODE), and the rotational degrees of freedom (1st order ODE)[66] based on the Evans-Murad quaternion formalism[67] involving a time-step size of 1.0 fs.

All interactions were truncated at a cutoff radius $r_c = \min(0.5\ L, 10$ Å), under standard 3D periodic boundary conditions so that each molecule interacts with the nearest-images of all the other molecules, and the van der Waals configurational properties were corrected by the corresponding long-range contributions assuming uniform density distributions for distances $r > r_c$ (see Appendix D in the Supporting Information of ref 40 for details). To solve self-consistently the implicit eq 12, we applied either the first-order predictor-iterative method proposed by Ahlström et al.[19] in the reaction-field implementation, or the $k = 2$ version of Kolafa's Always Stable Predictor–Corrector (ASPC) method[68] for the Ewald summation implementation, under the convergence criterion given by $\max(\mu_i^{\mathrm{ind(new)}} - \mu_i^{\mathrm{ind(old)}}) \le 5 \times 10^{-5}$ D. Note that, as discussed by Kiss and Baranyai,[69] this level of convergence is required since this correlates with the accuracy of the resulting system pressure.

Isochoric-isothermal MC involving $N = 256$ and isochoric GEMC simulations involving $255 \le N \le 400$ GCP water molecules were performed to determine the orthobaric conditions of the GCOS version of the original model, as well other properties that characterize its polarization behavior, in order to confront these results against those from the original GCP model. The present GEMC implementation involves the use of the recent MPM approach[39] to molecular translations and rotations, while volume changes and molecular transfer between phases followed standard implementations.[70] In fact, a typical run comprises 10^7 MC equilibration steps followed by 4×10^7 additional MC production steps, where each step consists of either a volume change, a particle exchange, the MPM translation of all particles in both simulation boxes, or the MPM rotation of all particles in both simulation boxes according to the probabilities 0.3–0.4 to 0.15–0.15, respectively.

The computationally efficient MPM-MC approach moves all the molecules simultaneously; first it translates all molecules within a particular simulation box (phase) in the direction of the corresponding center of mass forces, $\boldsymbol{f}_i (i = 1,N)$ and then adds a randomly chosen secondary translation to each molecule with Cartesian component γ chosen from Gaussian distributions, that is,

$$\boldsymbol{t}_i^\gamma = \beta p \boldsymbol{f}_i^{\gamma,\mathrm{old}} + \mathcal{R}_i^\gamma \tag{22}$$

where $\beta = 1/kT$, and $\mathcal{R}_i^\gamma$ is a random translational number characterized by a zero mean whose variance $\langle \mathcal{R}_i^\gamma \rangle = 2p$ can be adjusted by the parameter p. The acceptance probability for this MPM step is given by the following transition matrix elements:[39]

$$\omega^{\mathrm{old}\to\mathrm{new}} = (4p\pi)^{3N/2} \prod_{i=1}^{N} \exp[(-\beta p \boldsymbol{f}_i^{\mathrm{old}} - \mathbf{t}_i)^2]/4p$$
$$\omega^{\mathrm{new}\to\mathrm{old}} = (4p\pi)^{3N/2} \prod_{i=1}^{N} \exp[(-\beta p \boldsymbol{f}_i^{\mathrm{new}} - \mathbf{t}_i)^2]/4p \tag{23}$$

which can be conveniently recast in terms of the summation of the exponential arguments as follows:

$$\sum^{\mathrm{old}\to\mathrm{new}} = -\sum_{i=1}^{N} (\beta p \boldsymbol{f}_i^{\mathrm{old}} - \boldsymbol{t}_i)^2/4p$$
$$\sum^{\mathrm{new}\to\mathrm{old}} = -\sum_{i=1}^{N} (\beta p \boldsymbol{f}_i^{\mathrm{new}} + \boldsymbol{t}_i)^2/4p \tag{24}$$

Thus, the actual criterion for the acceptance of the MPM step becomes

$$\text{probability} = \min\left\{1, \exp\left(-\beta\Delta U + \sum^{\mathrm{new}\to\mathrm{old}} - \sum^{\mathrm{old}\to\mathrm{new}}\right)\right\} \tag{25}$$

where $\Delta U = U^{\mathrm{new}} - U^{\mathrm{old}}$ describes the change in configurational energy for the attempted move. Likewise, the MPM rotational step moves simultaneously all molecules within a particular phase around a vector $\boldsymbol{r}_i^\gamma = \beta \mathcal{T} \tau_i^{\gamma,\mathrm{old}} + \mathcal{R}_i^\gamma$ going

DOI: 10.1021/acs.jpcb.5b00595
J. Phys. Chem. B 2015, 119, 5010–5019

through a relevant molecular site (e.g., the center of mass), whose magnitude defines the angle of rotation, where the adjustable rotational parameter $\mathcal{T}$ is associated with the variance $\langle \mathcal{R}_i^{\gamma} \rangle = 2\mathcal{T}$, and τ_i^{γ} denotes the γ-component of the acting torque on the i-molecule. Thus, the elements of the transition matrix and acceptance probability for the rotational move are similar to those for the translation move, eqs 23−25, where we replace $[\beta p f_i^{\text{old}}, \beta p f_i^{\text{new}}]$ with $[\beta \mathcal{T} \tau_i^{\gamma,\text{old}}, \beta \mathcal{T} \tau_i^{\gamma,\text{new}}]$.

While the configurational energies and electric fields required in the GCOS electrostatic calculations are accurately determined using the full Ewald summation representation, the forces and torques for the MPM transition matrices are assessed following a faster reaction field approach,[39] rendering a more efficient algorithm without affecting the resulting thermophysical properties. Moreover, the condition of equilibrium for the Drude oscillators, eq 15, is determined by the usual iterative approach, starting with all Drude charges at their equilibrium positions, that is, $\{l_{\alpha_i} = 0;\ \alpha_i = 1, 2;\ i = 1, N\}$ with $q_{\text{D}_i}^{(\alpha)} = -q_{\text{D}_j}^{(\alpha)} = 10e$, so that at each iteration step we calculate the electric field $\boldsymbol{E}_{i_\alpha}^{\text{tot}}(\{\boldsymbol{\mu}_{i=1,N}^{\text{ind}}\})$ for the current position l_{α_i} and update it following an iterative optimization of eq 16 until we satisfy the convergence criterion $\max(l_{\alpha_i}^{\text{new}} - l_{\alpha_i}^{\text{old}}) \leq 10^{-4}$ Å.

IV. SIMULATION RESULTS AND DISCUSSION

In order to assess the equivalence between the two simulation implementations we performed the analysis of reliability by first determining the vapor−liquid phase coexistence envelope of the GCP model according to the GCOS within the interval $430 \leq T(K) \leq 610$ and compared it against that previously reported in our original SCF version,[59] as illustrated in Figure 2a,b. Note that while the VLE envelope in ref 59 is for the GCP water model whose electrostatic interactions were handled by a reaction field approach (see Appendix E of ref 40), we have recently shown its accuracy against the corresponding Ewald summation implementation for the description of the thermodynamic, microstructural, and polarization behavior of water over wide ranges of state conditions.[40] Thus, the observed agreement between the GCOS and the SCF calculations of the orthobaric state conditions attests to the equivalence between the two approaches for the molecular simulation of the GCP water model.

Obviously, the equivalence in the description of the VLE behavior points to a common root, that is, analogous polarization behavior as highlighted by Figure 3a,b, where we plot the behavior of the total and induced-dipole moments along the liquid branch of the orthobaric curve, based on the GCOS and SCF implementations. There are two common feature in these plots, namely, (a) the consistency between the results from the two induced polarization approaches and (b) the linearity not only for the $\boldsymbol{\mu}_{\text{tot}}(T_\sigma)$ and $\boldsymbol{\mu}_{\text{ind}}(T_\sigma)$ representations, where T_σ denotes the coexistence temperature (Figure 3a), but also for the $\boldsymbol{\mu}_{\text{tot}}[\boldsymbol{\mu}_{\text{ind}}(T_\sigma)]$ dependence (Figure 3b).

To find the origin of such a behavior we first invoke the vectorial nature of the dipole moments, that is, $\boldsymbol{\mu}_{\text{tot}} = \boldsymbol{m} + \boldsymbol{\mu}_{\text{ind}}$, where $\boldsymbol{\mu}_{\text{tot}} = |\boldsymbol{\mu}_{\text{tot}}|$, $m = |\boldsymbol{m}| \simeq 1.85$ D, and $\mu_{\text{ind}} = |\boldsymbol{\mu}_{\text{ind}}|$ denote the magnitude of the total, permanent, and induced dipole moments, respectively. Then, we analyze the corresponding behavior of the average value of the angle between the induced and permanent components of the dipole moment, that is, $\vartheta = \cos^{-1}(\boldsymbol{m}\cdot\boldsymbol{\mu}_{\text{ind}}/m\mu_{\text{ind}})$, as depicted in Figure 4a,b. These figures indicate that, on average, the permanent and induced dipole moments of a water molecule are not collinear, and that the average ϑ exhibits a rather strong dependence on μ_{ind} along the

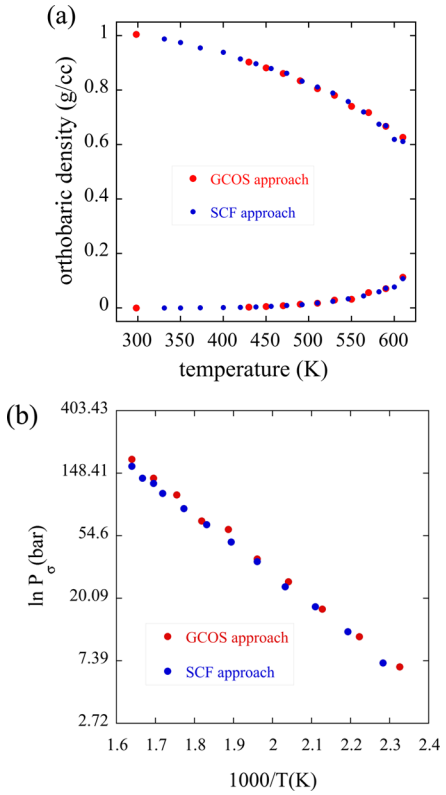

Figure 2. (a) Vapor−liquid equilibrium envelope and (b) saturation pressure P_σ of the GCP water model (ref 59) in comparison with that from the GCOS implementation.

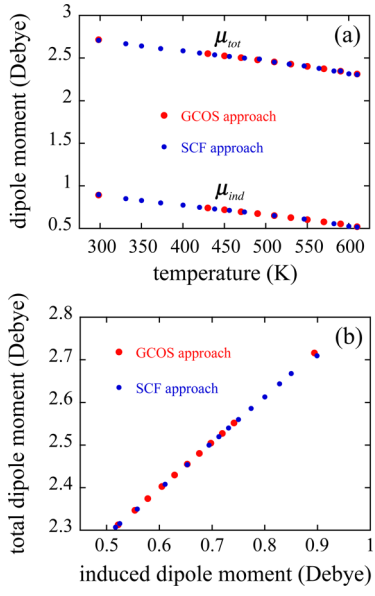

Figure 3. Magnitude of the total dipole moment $\boldsymbol{\mu}_{\text{tot}}$ and its corresponding induced dipole counterpart $\boldsymbol{\mu}_{\text{ind}}$ along the liquid branch of the vapor−liquid equilibrium envelope of the GCP water model (ref 59) in comparison with those from the GCOS implementation: (a) temperature dependence of $\boldsymbol{\mu}_{\text{tot}}$ (T_σ) and $\boldsymbol{\mu}_{\text{ind}}$ (T_σ), and (b) linear dependence between $\boldsymbol{\mu}_{\text{tot}}$ (T_σ) and $\boldsymbol{\mu}_{\text{ind}}$ (T_σ).

DOI: 10.1021/acs.jpcb.5b00595
J. Phys. Chem. B 2015, 119, 5010−5019

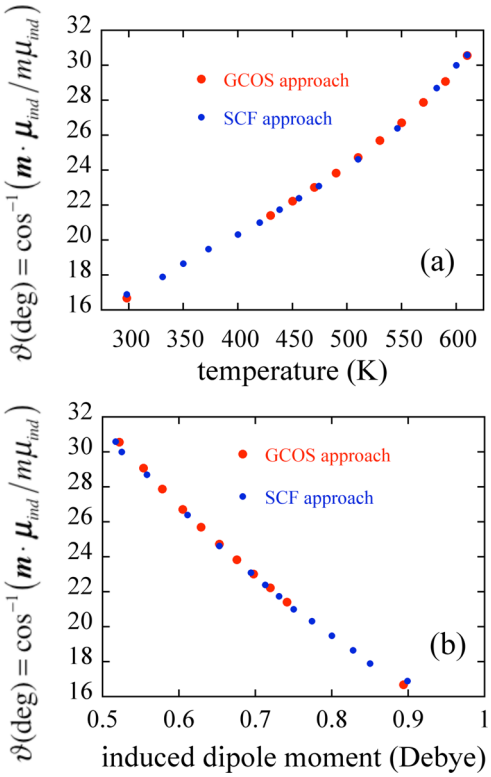

Figure 4. Magnitude of the angle $\vartheta = \cos^{-1}(\boldsymbol{\mu}_{perm} \times \boldsymbol{\mu}_{ind}/|\boldsymbol{\mu}_{perm}||\boldsymbol{\mu}_{ind}|)$ along the liquid branch of the vapor−liquid equilibrium envelope of the GCP water model (ref 59) in comparison with those from the GCOS implementation: (a) temperature dependence $\vartheta(T_\sigma)$, and (b) dependence between $\vartheta(T_\sigma)$ and $\boldsymbol{\mu}_{ind}(T_\sigma)$.

coexistence envelope under the obvious limiting condition $\lim_{\rho\to 0} \mu_{ind} = 0$, and consequently, $\lim_{\rho\to 0} \vartheta = 0°$.

To rationalize the linearity depicted in Figure 3b we draw a schematic in Figure 5 that illustrates the geometric links

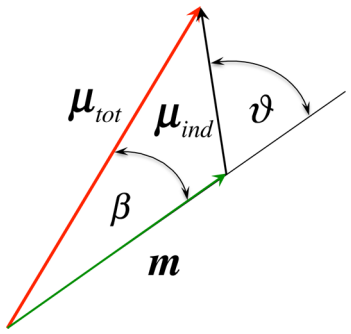

Figure 5. Relation between the $\angle\vartheta$, $\angle\beta$ and the magnitude of the two components of the total dipole moment.

between the two components of the total dipole moment of water. From that we can express the dot product $\boldsymbol{m}\cdot\boldsymbol{\mu}_{ind}$ as follows:

$$\boldsymbol{m}\cdot\boldsymbol{\mu}_{ind} = m\mu_{ind}\cos\vartheta$$
$$= \mathbf{m}\cdot(\boldsymbol{\mu}_{tot} - \boldsymbol{m}) = m\mu_{tot}\cos\beta - m^2 \quad (26)$$

from which we immediately have that

$$\mu_{tot} = m/\cos\beta + \mu_{ind}(\cos\vartheta/\cos\beta) \quad (27)$$

Because, typically, $\vartheta \geq \beta$ and $\cos\vartheta/\cos\beta \approx 1.0$, the observed compensation between the magnitude of ϑ and μ_{ind} in Figure 4b allows us to approximate eq 27 as $\mu_{tot}(\mathrm{D}) \approx a(T) + b(T)\mu_{ind}$ (D). We have previously found that for GCP water at extreme conditions, that is, $773 \leq T$ (K) ≤ 1373 and $10^{-4} \leq P$ (GPa) ≤ 20, $b(T) \approx 1.0$ and $a(T) \sim 1.7$ with regression coefficients $R > 0.9997$.[20] Interestingly, we find a similar dependence for GCP water along its coexistence envelope, that is, μ_{tot} (D) $\approx 1.75 + 1.07\ \mu_{ind}$ (D), a behavior that bears a direct connection with the variation of the strength of the hydrogen bond network as we addressed elsewhere.[20]

Finally, in Figures 6−8, we display the comparison of the simulated water microstructure, in terms of the three site−site

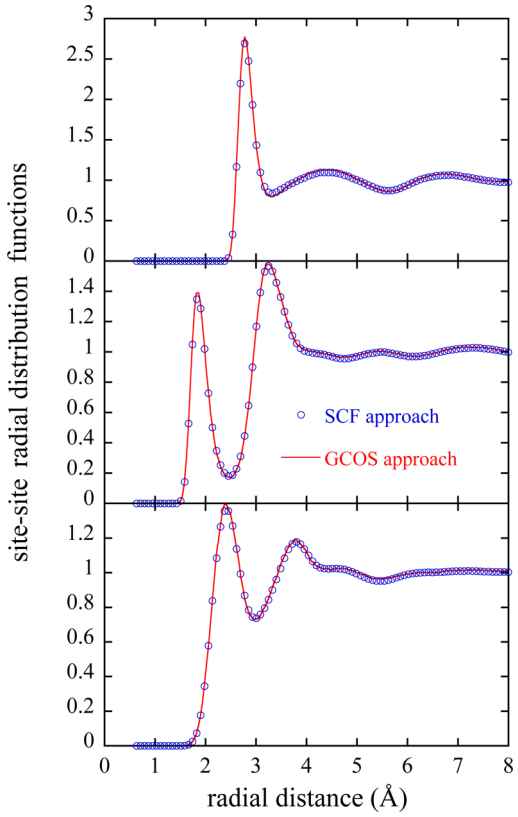

Figure 6. Microstructure of GCP model water at ambient conditions. Comparison of the site−site radial distribution functions from SCF and GCOS implementations.

pair radial distribution functions, resulting from the implementation of the GCOS and SCF approaches to polarization induction. For this comparison we chose three state conditions along the liquid branch of the coexistence curve, that is, ambient, (474 K, 0.862 g/cc) and (610 K, 0.612 g/cc). The three sets of radial distribution functions provide a clear evidence for the equivalence between the two polarization approaches in the description of the water microstructure. Moreover, from a polarization standpoint, these distribution functions illustrate the significant transformation of the original hydrogen bonded network at ambient conditions as the system moves toward criticality along the liquid branch of the orthobaric curve. This transformation can be characterized by a number of hydrogen bonds per water molecule $n_{HB}(r^{\otimes}_{OH}) = 4\pi\rho_H \int_{0}^{r^{\otimes}_{OH}} g_{OH}(r) r^2 dr$, where $r^{\otimes}_{OH}$ locates the first valley of $g_{OH}(r)$, and ρ_H defines the atomic density of water hydrogen sites consistent with the system's state conditions.[71] Alter-

DOI: 10.1021/acs.jpcb.5b00595
J. Phys. Chem. B 2015, 119, 5010−5019

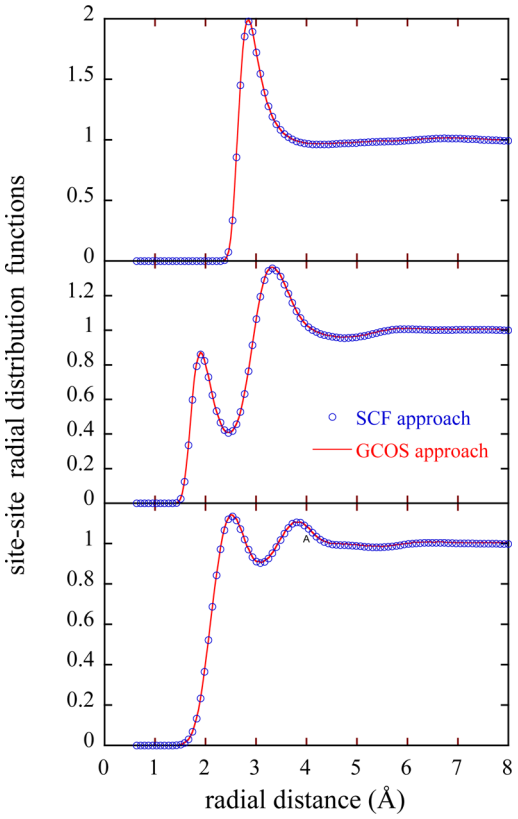

Figure 7. Microstructure of GCP model water at the orthobaric condition of 474 K and 0.862 g/cc. Comparison of site−site radial distribution functions from SCF and GCOS implementations.

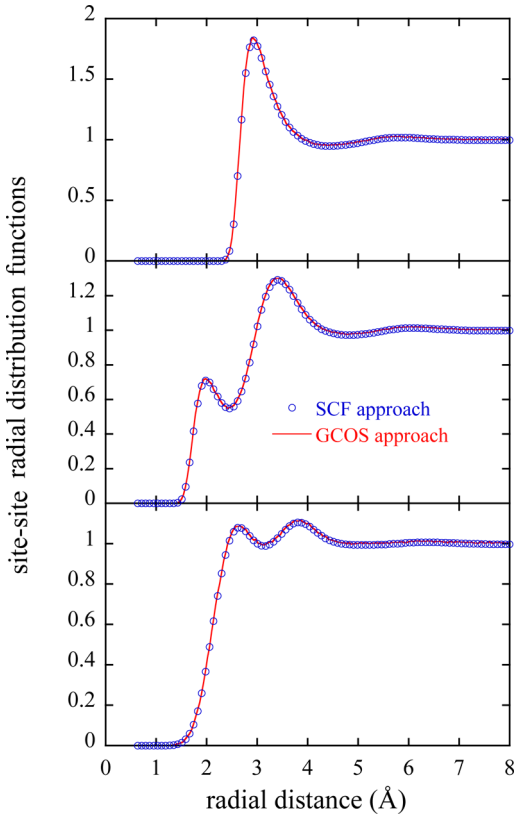

Figure 8. Microstructure of GCP model water at the orthobaric condition 610 K and 0.612 g/cc. Comparison of site−site radial distribution functions from SCF and GCOS implementations.

natively, this evolution can be done according to Wernet et al.'s $R-\beta$ geometric criterion, with R (Å) = 3.3−0.00044 β^2, where R is the O···O to the nearest water neighbors, and β is the ∠O···O−H in degrees.[72] In Table 1 we summarize this behavior complemented by the corresponding magnitude of the induced dipole moments.

Table 1 illustrates the direct link between the strength of hydrogen bonding and the corresponding magnitude of the induced dipole moment, while the companion Figure 9 provides additional support to that contention, where we include additional simulation data along the liquid branch of the coexistence envelope. From the comparison in Figure 9 it becomes evident that the number of hydrogen bonds under Wernet et al.'s geometric description is well represented by a monotonic increasing function of the magnitude of the average induced dipole moment of water over a wide range of state conditions regardless of either temperature or density. In fact, for this range of induced dipole moments, that is, $0.50 \leq \mu_{ind} \leq 0.90$, we find a similar linear dependence to that observed over a much wider temperature range (e.g., Figure 8b of ref 20), a behavior that points to a representation with a negligible temperature dependence.

Table 1. Evolution of the Hydrogen Bonding along the Orthobaric Curve

T_σ (K)	ρ (g/cc)	n_{HB} ($r_{OH}^{\otimes}$)	n_{HB} (R,β)	μ_{ind} (D)
298	0.997	3.8	3.3	0.89
474	0.862	3.0	2.2	0.69
610	0.612	2.2	1.27	0.52

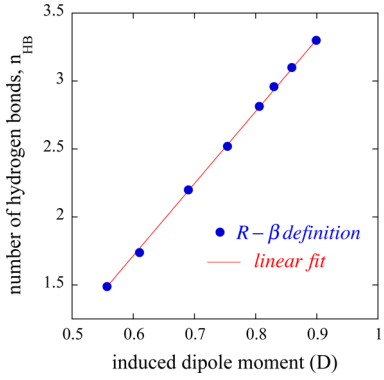

Figure 9. Number of hydrogen bonds per molecule according to the $R-\beta$ description as a function of the average induced dipole moment.

V. FINAL REMARKS

An important element in the charge-on-spring implementation is the judicious choice of the magnitude of the Drude charge q_D, which in turn will fix the spring's force constant k_D for a given site dipolar polarizability. While this choice for point charges has been often based on stability issues,[73] here we invoke the SCF induction response as a suitable reference to analyze the convergence and stability of the GCOS response. More specifically, in Figure 10a,b, we illustrate the magnitude of the energy deviation, ΔU, between the GCOS and the SCF representations of the Gaussian charge-induced dipole interactions as a function of Gaussian width, $\sigma = (\kappa\sqrt{2})^{-1}$, and the Drude charge, q_D. For this illustration, we use the gas phase dipole polarizability of water, α = 1.444 Å, and a

DOI: 10.1021/acs.jpcb.5b00595
J. Phys. Chem. B 2015, 119, 5010−5019

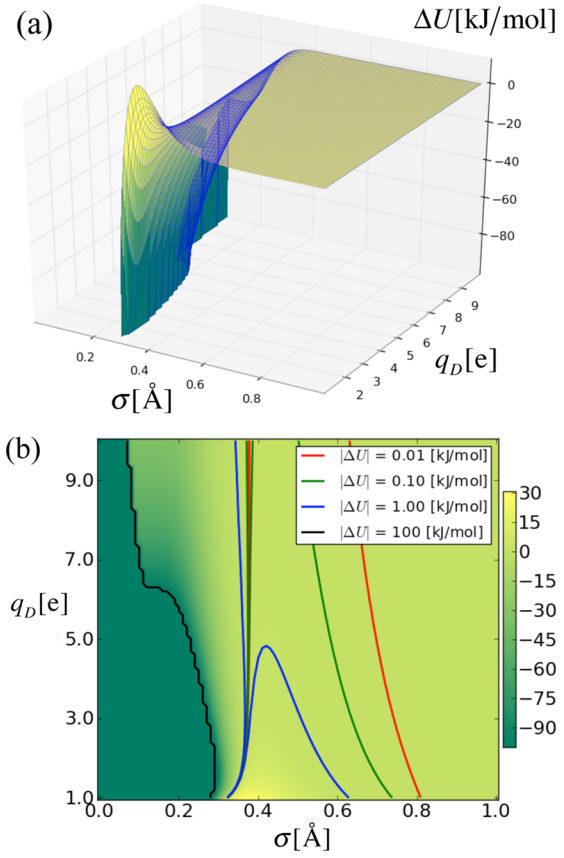

Figure 10. Configurational energy deviation, ΔU, between the GCOS and the SCF representations for the Gaussian charge-induced dipole interactions as a function of the Gaussian width, σ, and the Drude charge, q_D: (a) 3D surface and (b) 2D parameteric representations.

representative distance between the center of the induced dipole and the Gaussian charge, that is, 1.0 Å, which can be considered a realistic lower limit of nonbonded particle−particle separations encountered in the simulations of aqueous systems.[74] The line contours in Figure 10b locate the regions of the $\sigma-q_D$ parameter space that guarantee energy deviations smaller than the specified values. For instance, for a representative width σ = 0.5 Å, and a Drude charge $q_D = 10e$ we will encounter energy deviations (errors) smaller than $0.10RT$ kJ/mol even at extremely short Gaussian charge-induced dipole separations. Moreover, as the Gaussian charge width decreases toward the point charge limit, Figure 10a,b suggest that the combination of narrower Gaussian charge widths and smaller Drude charges will increase the chances for catastrophic deviations (errors).

For the current study of the GCP water model involving $2 \leq q_D(e) \leq 10$ we have observed no differences in the thermodynamics, microstructural, and polarization quantities according to the GCOS and SCF approaches to induced polarization. In principle and according to Figure 10a,b, the larger the q_D, the better the GCOS description of the SCF induced dipole moment of the GCP water model. The use of the proposed GCOS alternative to the original SCF implementation of the GCP water model might facilitate the incorporation of this model into molecular simulation packages, and will obviously simplify the adaptation of recently developed simulation algorithms for the study of ionic clusters[75] and solubility phenomena involving ionic compounds[76] based on GCP modeling. In fact, we are currently implementing the GCOS methodology in the highly scalable LAMMPS simulation package[77] by incorporating the Gaussian charge interaction as a new pair style where the COS functionality is achieved through the use of existing harmonic bond interactions and iterative energy minimization procedures.

AUTHOR INFORMATION

Corresponding Author

*E-mail: chialvoaa@ornl.gov. Fax: 865-574-4961.

Notes

The authors declare no competing financial interest.

ACKNOWLEDGMENTS

This research was supported by the U.S. Department of Energy, Office of Science, Basic Energy Sciences, Chemical Sciences, Geosciences, and Biosciences Division. The participation of F.M. and I.N. was facilitated by the Czech−U.S.A. cooperative research program *Nonadditive Interactions in Aqueous Solutions of Electrolytes*. This manuscript has been authored by UT-Battelle, LLC under Contract No. DE-AC05-00OR22725 with the U.S. Department of Energy. The United States Government retains and the publisher, by accepting the article for publication, acknowledges that the United States Government retains a nonexclusive, paid-up, irrevocable, worldwide license to publish or reproduce the published form of this manuscript, or allow others to do so, for United States Government purposes. The Department of Energy will provide public access to these results of federally sponsored research in accordance with the DOE Public Access Plan (http://energy.gov/downloads/doe-public-access-plan).

REFERENCES

(1) Ben-Naim, A.; Stillinger, F. H. Water and Aqueous Solutions. In *Structure and Transport of Processes in Water and Aqueous Solutions*; Horne, R. A., Ed.; Wiley-Interscience: New York, 1972.

(2) Chialvo, A. A.; Cummings, P. T. Molecular-Based Modeling of Water and Aqueous Solutions at Supercritical Conditions. *Adv. Chem. Phys.*; John Wiley & Sons Inc: New York, 1999; Vol. *109*, pp 115−205.

(3) Wallqvist, A.; Mountain, R. D. Molecular Models of Water: Derivation and Description. *Rev. Comput. Chem.* **1999**, *13*, 183−247.

(4) Guillot, B. A Reappraisal of What We Have Learnt During Three Decades of Computer Simulations on Water. *J. Mol. Liq.* **2002**, *101*, 219−260.

(5) Baranyai, A.; Bartok, A.; Chialvo, A. A. Limitations of the Rigid Planar Non-Polarizable Models of Water. *J. Chem. Phys.* **2006**, *124*, No. 074507.

(6) Chialvo, A. A.; Bartok, A.; Baranyai, A. On the Re-Engineered Tip4p Water Models for the Predictions of Vapor-Liquid Equilibrium. *J. Mol. Liq.* **2006**, *129*, 120−124.

(7) Vega, C.; Abascal, J. L. F. Simulating Water with Rigid Non-Polarizable Models: A General Perspective. *Phys. Chem. Chem. Phys.* **2011**, *13*, 19663−19688.

(8) Fuentes-Azcatl, R.; Alejandre, J. Non-Polarizable Force Field of Water Based on the Dielectric Constant: Tip4p/E. *J. Phys. Chem. B* **2014**, *118*, 1263−1272.

(9) Shi, L.; Ni, Y.; Drews, S. E. P.; Skinner, J. L. Dielectric Constant and Low-Frequency Infrared Spectra for Liquid Water and Ice Ih within the E3b Model. *J. Chem. Phys.* **2014**, *141*, No. 084508.

(10) Leontyev, I. V.; Stuchebrukhov, A. A. Electronic Polarizability and the Effective Pair Potentials of Water. *J. Chem. Theor. Comp.* **2010**, *6*, 3153−3161.

(11) Fuentes-Azcatl, R.; Mendoza, N.; Alejandre, J. Improved Spc Force Field of Water Based on the Dielectric Constant: Spc. *Phys. A (Amsterdam, Neth.)* **2015**, *420*, 116−123.

DOI: 10.1021/acs.jpcb.5b00595
J. Phys. Chem. B 2015, 119, 5010−5019

(12) Chipman, D. M. Water from Ambient to Supercritical Conditions with the Amoeba Model. *J. Phys. Chem. B* **2013**, *117*, 5148−5155.
(13) Ponder, J. W.; Wu, C. J.; Ren, P. Y.; Pande, V. S.; Chodera, J. D.; Schnieders, M. J.; Haque, I.; Mobley, D. L.; Lambrecht, D. S.; DiStasio, R. A.; et al. Current Status of the Amoeba Polarizable Force Field. *J. Phys. Chem. B* **2010**, *114*, 2549−2564.
(14) Wang, L.-P.; Head-Gordon, T.; Ponder, J. W.; Ren, P.; Chodera, J. D.; Eastman, P. K.; Martinez, T. J.; Pande, V. S. Systematic Improvement of a Classical Molecular Model of Water. *J. Phys. Chem. B* **2013**, *117*, 9956−9972.
(15) Troster, P.; Lorenzen, K.; Schworer, M.; Tavan, P. Polarizable Water Models from Mixed Computational and Empirical Optimization. *J. Phys. Chem. B* **2013**, *117*, 9486−9500.
(16) Lamoureux, G.; MacKerell, A. D.; Roux, B. A Simple Polarizable Model of Water Based on Classical Drude Oscillators. *J. Chem. Phys.* **2003**, *119*, 5185−5197.
(17) Dang, L. X.; Chang, T. M. Molecular Dynamics Study of Water Clusters, Liquid, and Liquid-Vapor Interface of Water with Many-Body Potentials. *J. Chem. Phys.* **1997**, *106*, 8149−8159.
(18) Chialvo, A. A.; Cummings, P. T. Engineering a Simple Polarizable Model for the Molecular Simulation of Water Applicable over Wide Ranges of State Conditions. *J. Chem. Phys.* **1996**, *105*, 8274−8281.
(19) Ahlström, P.; Wallqvist, A.; Engström, S.; Jönsson, B. A Molecular Dynamics Study of Polarizable Water. *Mol. Phys.* **1989**, *68*, 563−581.
(20) Chialvo, A. A.; Horita, J. Polarization Behavior of Water in Extreme Aqueous Environments: A Molecular Dynamics Study Based on the Gaussian Charge Polarizable Water Model. *J. Chem. Phys.* **2010**, *133*, No. 074504.
(21) Alejandre, J.; Tildesley, D. J.; Chapela, G. A. Molecular-Dynamics Simulation of the Orthobaric Densities and Surface-Tension of Water. *J. Chem. Phys.* **1995**, *102*, 4574−4583.
(22) Gelb, L. D.; Muller, E. A. Location of Phase Equilibria by Temperature-Quench Molecular Dynamics Simulations. *Fluid Phase Equilib.* **2002**, *203*, 1−14.
(23) Errington, J. R.; Panagiotopoulos, A. Z. A Fixed Point Charge Model for Water Optimized for the Vapor-Liquid Coexistence Properties. *J. Phys. Chem. B* **1998**, *102*, 7470−7475.
(24) Panagiotopoulos, A. Z. Monte Carlo Methods for Phase Equilibria of Fluids. *J. Phys.: Condens. Matter* **2000**, *12*, R25−R52.
(25) Palmer, B. J.; Lo, C. M. Molecular-Dynamics Implementation of the Gibbs Ensemble Calculation. *J. Chem. Phys.* **1994**, *101*, 10899−10907.
(26) Ouyang, W. Z.; Lu, Z. Y.; Sun, Z. Y.; An, L. J. Molecular Dynamics Study on the Phase Diagrams of Linear and Branched Chain Molecules. *Chem. Phys.* **2008**, *344*, 52−60.
(27) Ramana, A. S. V. Molecular Dynamics Simulation of Liquid-Vapor Coexistence Curves of Metals. 23rd International Conference on High Pressure Science and Technology (Airapt-23). *J. Phys.: Conf. Ser.* **2012**, *377*, 012086.
(28) Baranyai, A.; Cummings, P. T. On the Molecular Dynamics Algorithm for Gibbs Ensemble Simulation. *Mol. Simul.* **1996**, *17*, 21−25.
(29) Kofke, D. A. Gibbs-Duhem Integration: A New Method for the Direct Evaluation of Phase Coexistence by Molecular Simulation. *Mol. Phys.* **1993**, *78*, 1331−1336.
(30) Medeiros, M.; Costas, M. E. Gibbs Ensemble Monte Carlo Simulation of the Properties of Water with a Fluctuating Charges Model. *J. Chem. Phys.* **1997**, *107*, 2012−2019.
(31) Chen, B.; Siepmann, J. I. Monte Carlo Algorithms for Simulating Systems with Adiabatic Separation of Electronic and Nuclear Degrees of Freedom. *Theor. Chem. Acc.* **1999**, *103*, 87−104.
(32) Predota, M.; Chialvo, A. A.; Cummings, P. T. On the Determination of the Vapor-Liquid Envelope for Polarizable Models by Monte Carlo Simulation. *Fluid Phase Equilib.* **2001**, *183*, 295−300.
(33) Chen, B.; Potoff, J. J.; Siepmann, J. I. Adiabatic Nuclear and Electronic Sampling Monte Carlo Simulations in the Gibbs Ensemble: Application to Polarizable Force Fields for Water. *J. Phys. Chem. B* **2000**, *104*, 2378−2390.
(34) Predota, M.; Cummings, P. T.; Chialvo, A. A. New Approximate Method for Efficient Monte Carlo Simulations of Polarizable Fluids. *Mol. Phys.* **2001**, *99*, 349−354.
(35) Predota, M.; Cummings, P. T.; Chialvo, A. A. Pair Approximation for Polarization Interaction and Adiabatic Nuclear and Electronic Sampling Method for Fluids with Dipole Polarizability. *Mol. Phys.* **2002**, *100*, 2703−2717.
(36) Moucka, F.; Rouha, M.; Nezbeda, I. Efficient Multiparticle Sampling in Monte Carlo Simulations on Fluids: Application to Polarizable Models. *J. Chem. Phys.* **2007**, *126*, No. 224106.
(37) Moucka, F.; Nezbeda, I. Multi-Particle Sampling in Monte Carlo Simulations on Fluids: Efficiency and Extended Implementations. *Mol. Simul.* **2009**, *35*, 660−672.
(38) Moucka, F.; Nezbeda, I. Gibbs Ensemble Simulation on Polarizable Models: Vapor-Liquid Equilibrium in Baranyai-Kiss Models of Water. *Fluid Phase Equilib.* **2013**, *360*, 472−476.
(39) Moucka, F.; Nezbeda, I.; Smith, W. R. Computationally Efficient Monte Carlo Simulations for Polarisable Models: Multi-Particle Move Method for Water and Aqueous Electrolytes. *Mol. Simul.* **2013**, *39*, 1125−1134.
(40) Chialvo, A. A.; Vlcek, L. Ewald Summation Approach to Potential Models of Aqueous Electrolytes Involving Gaussian Charges and Induced Dipoles: Formal and Simulation Results. *J. Phys. Chem. B* **2014**, *118*, 13658−13670.
(41) Kirkwood, J. G. The Dielectric Polarization of Polar Liquids. *J. Chem. Phys.* **1939**, *7*, 911−919.
(42) Onsager, L. Electric Moments of Molecules in Liquids. *J. Am. Chem. Soc.* **1936**, *58*, 1486−1493.
(43) Rick, S. W.; Stuart, S. J. Potentials and Algorithms for Incorporating Polarizability in Computer Simulations. In *Reviews in Computational Chemistry*; Lipkowitz, K. B., Boyd, D. B., Eds.; Wiley-VCH, Inc.: New York, 2002; Vol. *18*, pp 89−146.
(44) Cieplak, P.; Dupradeau, F. Y.; Duan, Y.; Wang, J. M. Polarization Effects in Molecular Mechanical Force Fields. *J. Phys.: Condens. Matter* **2009**, *21*, No. 333102.
(45) Halgren, T. A.; Damm, W. Polarizable Force Fields. *Curr. Opin. Struct. Biol.* **2001**, *11*, 236−242.
(46) Straatsma, T. P.; McCammon, J. A. Molecular Dynamics Simulations with Interaction Potentials Including Polarization Development of a Noniterative Method and Application to Water. *Mol. Simul.* **1990**, *5*, 181−192.
(47) Yu, H. B.; Hansson, T.; van Gunsteren, W. F. Development of a Simple, Self-Consistent Polarizable Model for Liquid Water. *J. Chem. Phys.* **2003**, *118*, 221−234.
(48) Lamoureux, G.; Roux, B. Modeling Induced Polarization with Classical Drude Oscillators: Theory and Molecular Dynamics Simulation Algorithm. *J. Chem. Phys.* **2003**, *119*, 3025−3039.
(49) Jacucci, G.; McDonald, I. R.; Singer, K. Introduction of Shell-Model of Ionic Polarizability into Molecular-Dynamics Calculations. *Phys. Lett. A* **1974**, *50*, 141−143.
(50) Pan, D.; Wan, Q.; Galli, G. The Refractive Index and Electronic Gap of Water and Ice Increase with Increasing Pressure. *Nat. Commun.* **2014**, *5*, No. 3919.
(51) Sahle, C. J.; et al. Microscopic Structure of Water at Elevated Pressures and Temperatures. *Proc. Natl. Acad. Sci. U.S.A.* **2013**, *110*, 6301−6306.
(52) Oostenbrink, C.; Villa, A.; Mark, A. E.; Van Gunsteren, W. F. A Biomolecular Force Field Based on the Free Enthalpy of Hydration and Solvation: The Gromos Force-Field Parameter Sets 53a5 and 53a6. *J. Comput. Chem.* **2004**, *25*, 1656−1676.
(53) Phillips, J. C.; Braun, R.; Wang, W.; Gumbart, J.; Tajkhorshid, E.; Villa, E.; Chipot, C.; Skeel, R. D.; Kale, L.; Schulten, K. Scalable Molecular Dynamics with Namd. *J. Comput. Chem.* **2005**, *26*, 1781−1802.
(54) Brooks, B. R.; Sternemann, C.; Schmidt, C.; Lehtola, S.; Jahn, S.; Simonelli, L.; Huotari, S.; Hakala, M.; Pylkkanen, T.; Nyrow, A.; et al.

DOI: 10.1021/acs.jpcb.5b00595
J. Phys. Chem. B 2015, 119, 5010−5019

Charmm: The Biomolecular Simulation Program. *J. Comput. Chem.* **2009**, *30*, 1545−1614.
(55) Todorov, I. T.; Smith, W.; Trachenko, K.; Dove, M. T. Dl_Poly_3: New Dimensions in Molecular Dynamics Simulations Via Massive Parallelism. *J. Mater. Chem.* **2006**, *16*, 1911−1918.
(56) Baranyai, A.; Kiss, P. T. A Transferable Classical Potential for the Water Molecule. *J. Chem. Phys.* **2010**, *133*, 144109.
(57) Kiss, P. T.; Sega, M.; Baranyai, A. Efficient Handling of Gaussian Charge Distributions: An Application to Polarizable Molecular Models. *J. Chem. Theory Comput.* **2014**, *10*, 5513−5519.
(58) Chialvo, A. A.; Cummings, P. T. Simple Transferable Intermolecular Potential for the Molecular Simulation of Water over Wide Ranges of State Conditions. *Fluid Phase Equilib.* **1998**, *150−151*, 73−81.
(59) Paricaud, P.; Predota, M.; Chialvo, A. A.; Cummings, P. T. From Dimer to Condensed Phases at Extreme Conditions: Accurate Predictions of the Properties of Water by a Gaussian Charge Polarizable Model. *J. Chem. Phys.* **2005**, *122*, No. 244511.
(60) Chialvo, A. A.; Horita, J. Liquid−Vapor Equilibrium Isotopic Fractionation of Water: How Well Can Classical Water Models Predict It? *J. Chem. Phys.* **2009**, *130*, No. 094509.
(61) Hirschfelder, J. O.; Curtiss, C. F.; Bird, R. B. *Molecular Theory of Gases and Liquids*; Wiley and Son, Inc.: New York, 1954.
(62) Ruocco, G.; Sampoli, M. Computer-Simulation of Polarizable Fluids: A Consistent and Fast Way for Dealing with Polarizability and Hyperpolarizability. *Mol. Phys.* **1994**, *82*, 875−886.
(63) Gray, C. G.; Gubbins, K. E. *Theory of Molecular Fluids*; Oxford University Press: New York, 1985; Vol. *1*.
(64) Nosé, S. A Unified Formulation of the Constant Temperature Molecular Dynamics Methods. *J. Chem. Phys.* **1984**, *81*, 511−519.
(65) Nosé, S. A Molecular Dynamics Method for Simulations in the Canonical Ensemble. *Mol. Phys.* **1984**, *52*, 255−268.
(66) Gear, C. W. *The Numerical Integration of Ordinary Differential Equations of Various Orders, ANL-7126*; Argonne National Laboratory: Chicago, 1966.
(67) Evans, D. J.; Murad, S. Singularity Free Algorithm for Molecular Dynamics Simulation of Rigid Polyatomics. *Mol. Phys.* **1977**, *34*, 327−331.
(68) Kolafa, J. Time-Reversible Always Stable Predictor-Corrector Method for Molecular Dynamics of Polarizable Molecules. *J. Comput. Chem.* **2004**, *25*, 335−342.
(69) Kiss, P. T.; Baranyai, A. On the Pressure Calculation for Polarizable Models in Computer Simulation. *J. Chem. Phys.* **2012**, *136*, 104109−8.
(70) Frenkel, D.; Smit, B. *Understanding Molecular Simulation*, 2nd. ed.; Academic Press: London, 2002.
(71) Kumar, R.; Schmidt, J. R.; Skinner, J. L. Hydrogen Bonding Definitions and Dynamics in Liquid Water. *J. Chem. Phys.* **2007**, *126*.
(72) Wernet, P.; Nordlund, D.; Bergmann, U.; Cavalleri, M.; Odelius, M.; Ogasawara, H.; Naslund, L. A.; Hirsch, T. K.; Ojamae, L.; Glatzel, P.; Pettersson, L. G. M.; et al. The Structure of the First Coordination Shell in Liquid Water. *Science* **2004**, *304*, 995−999.
(73) Yu, H. B.; Whitfield, T. W.; Harder, E.; Lamoureux, G.; Vorobyov, I.; Anisimov, V. M.; MacKerell, A. D.; Roux, B. Simulating Monovalent and Divalent Ions in Aqueous Solution Using a Drude Polarizable Force Field. *J. Chem. Theory Comput.* **2010**, *6*, 774−786.
(74) Alfredsson, M.; Brodholt, J. P.; Hermanson, K.; Vallauri, R. The Use of a Point Polarizable Dipole in Intermolecular Potentials for Water. *Mol. Phys.* **1998**, *94*, 873−876.
(75) Vlcek, L.; Uhlik, F.; Moucka, F.; Nezbeda, I.; Chialvo, A. A. Thermodynamics of Small Alkali Halide Cluster Ions: Comparison of Classical Molecular Simulations with Experiment and Quantum Chemistry. *J. Phys. Chem. A* **2015**, *119*, 488−500.
(76) Moucka, F.; Lisal, M.; Skvor, J.; Jirsak, J.; Nezbeda, I.; Smith, W. R. Molecular Simulation of Aqueous Electrolyte Solubility. 2. Osmotic Ensemble Monte Carlo Methodology for Free Energy and Solubility Calculations and Application to Nacl. *J. Phys. Chem. B* **2011**, *115*, 7849−7861.
(77) Plimpton, S. Fast Parallel Algorithms for Short-Range Molecular-Dynamics. *J. Comput. Phys.* **1995**, *117*, 1−19.

DOI: 10.1021/acs.jpcb.5b00595
J. Phys. Chem. B 2015, 119, 5010−5019